

# III-Nitride Ultraviolet Photonic Materials – Epitaxial Growth, Optical and Electrical Properties, and Applications

J. Y. Lin and H. X. Jiang

Department of Physics, Kansas State University, Manhattan, KS 66506-2601

## ABSTRACT

This paper summarizes some of the recent advances made by our group on the growth, characterization and applications of AlGa<sub>x</sub>N alloys with high Al contents. Recently, our group has achieved highly conductive n-type Al<sub>x</sub>Ga<sub>1-x</sub>N for x as high as 0.7 (a resistivity value as low as 0.15 ohm-cm has been achieved). Prior to this, only insulating Al<sub>x</sub>Ga<sub>1-x</sub>N (x > 0.5) can be obtained. Our success is largely attributed to our unique capability for monitoring the optical qualities of these layers - the development of the world's first (and presently only) deep UV picosecond time-resolved optical spectroscopy system for probing the optical properties of III-nitrides [photoluminescence (PL), electro-luminescence (EL), etc.] with a time-resolution of a few ps and wavelength down to deep UV (down to 195 nm) [11]. Our time-resolved PL results have shown that we must fill in the localization states (caused by alloy fluctuation) by doping before conduction could occur. The density of states of localization states is about 10<sup>18</sup>/cm<sup>3</sup> in this system. It was also shown that Al<sub>x</sub>Ga<sub>1-x</sub>N alloys could be made n-type for x up to 1 (pure AlN). Time-resolved photoluminescence (PL) studies carried out on these materials have revealed that Si-doping reduces the effect of carrier localization in Al<sub>x</sub>Ga<sub>1-x</sub>N alloys and a sharp drop in carrier localization energy as well as a sharp increase in conductivity occurs when the Si doping concentration increases to above 1 x 10<sup>18</sup> cm<sup>-3</sup>. For the Mg-doped Al<sub>x</sub>Ga<sub>1-x</sub>N alloys, p-type conduction was achieved for x up to 0.27. The Mg acceptor activation energy as a function of Al content has been deduced. Mg-δ-doping in GaN and AlGa<sub>x</sub>N epilayers has been investigated. We have demonstrated that δ-doping significantly suppresses the dislocation density, enhances the p-type conduction, and reduces the non-radiative recombination centers in GaN and AlGa<sub>x</sub>N. AlN epilayers with high optical qualities have also been grown on sapphire substrates. Very efficient band-edge PL emission lines have been observed for the first time with above bandgap deep UV laser excitation. We have shown that the thermal quenching of the PL emission intensity is much less severe in AlN than in GaN and the optical quality of AlN can be as good as GaN. From the low temperature (10 K) emission spectra, as well as the temperature dependence of the recombination lifetime and the PL emission intensity, the binding energies of the bound excitons and free excitons in AlN were deduced to be around 16 meV and 80 meV, respectively. From this, the energy bandgap of AlN epilayers grown on sapphire was found to be around 6.11 eV at 10 K. The observed large free exciton binding energy implies that excitons in AlN are extremely robust entities. This together with other well-known physical properties of AlN may considerably expand future prospects for the application of III-nitride materials.

**Keywords:** Al<sub>x</sub>Ga<sub>1-x</sub>N, wide bandgap, time-resolved PL, optical transitions, UV light emitters

## 1. BACKGROUND

Ultraviolet (UV) light causes many fissionable materials and dangerous bacteria to fluoresce efficiently in the near UV and visible regions. In particular, there is currently a great need for solid-state UV emitters for the detection of chemical and biological agents. Al-rich AlGa<sub>x</sub>N alloys, covering wavelengths from 300 nm to 200 nm, are ideal materials for the development of chip-scale UV light sources/sensors, because AlGa<sub>x</sub>N is the only wide-bandgap semiconductor system which allows the bandgap engineering through the use of alloying and heterostructure design [1,2]. Efficient solid-state UV light sources/sensors are crucial for many other applications. For instance, protein fluorescence is generally excited by UV light; monitoring changes of intrinsic fluorescence in a protein can provide important information on its structural changes [3]. Hence, the availability of chip-scale UV light sources may open new avenues for medical research. On the other hand, the current approach for generating white light is by coating the InGa<sub>x</sub>N/GaN quantum well (QW) blue LED chips with yellow or green phosphor [4-9]. Through color mixing, the eye sees white when two colors are properly balanced. This approach however suffers from severe color rendering and low power conversion efficiency problems [10]. These problems can be greatly minimized by employing UV LEDs together with three-color phosphors for wavelength down conversion. Although many of the ideas and potentials of III-nitride devices for UV applications have been identified, a transition from basic

research to practical device components has not yet been made due to various technological obstacles. The attainment of highly conductive p-type AlGa<sub>x</sub>N (of any Al composition) and n-type Al<sub>x</sub>Ga<sub>1-x</sub>N alloys ( $x > 0.7$ ) remain one of the foremost challenging tasks of the Nitride community. This paper summarizes some of the recent advances made by our group on the growth and characterization of AlGa<sub>x</sub>N alloys with high Al contents.

## 2. EXPERIMENT

Al<sub>x</sub>Ga<sub>1-x</sub>N alloys and AlN epilayers (1 μm thick) were grown on sapphire (0001) substrates with AlN buffer layers by metal organic chemical vapor deposition (MOCVD). The growth temperature and pressure were around 1050 °C and 50 Torr, respectively. The metal organic sources used were trimethylgallium (TMGa) for Ga and trimethylaluminum (TMAI) for Al. For Mg-doping of AlGa<sub>x</sub>N, bis-cyclopentadienyl-magnesium (Cp<sub>2</sub>Mg) was transported into the growth chamber with ammonia during growth. The gas sources used were blue ammonia (NH<sub>3</sub>) for N and Silane (SiH<sub>4</sub>) for Si doping and the doping level was varied by controlling the SiH<sub>4</sub> flow rate. The Al contents of Al<sub>x</sub>Ga<sub>1-x</sub>N alloys were determined by energy dispersive x-ray (EDX) microanalysis and x-ray diffraction (XRD) measurement as well as by the flow rates of TMGa and TMAI. The Al contents ( $x$ ) determined by all three methods agreed within  $\pm 0.02$ . The Si-dopant concentrations were determined by the flow rate of SiH<sub>4</sub> as well as by the variable temperature Hall effect measurement at elevated temperatures ( $T < 650$  K). Additionally, secondary ion mass spectroscopy (SIMS) measurements were performed (by Charles and Evan) for selective samples to verify the Si-dopant concentrations. Atomic force microscopy (AFM) and scanning electron microscopy (SEM) were employed to examine the surfaces and revealed crack-free Al<sub>x</sub>Ga<sub>1-x</sub>N epilayers. Variable temperature Hall-effect (Standard Van der Pauw) measurements were employed to measure the electron concentration, mobility, and resistivity of these materials.

A deep UV (10 mW @ 196 nm) picosecond time-resolved photoluminescence (PL) spectroscopy system was specially designed to probe the optical properties of materials and device structures based on AlGa<sub>x</sub>N and InAlGa<sub>x</sub>N alloys with high Al contents and serves as “eyes” for monitoring the material qualities of these materials. The picosecond time-resolved PL spectroscopy system consists of a frequency quadrupled 100 femtosecond Ti: sapphire laser with a 76 MHz repetition rate, a monochromator (1.3 m), and a streak camera with a detection capability ranging from 185 – 800 nm and a time resolution of 2 ps [11]. For GaN-rich alloys, in addition to the 196 nm deep UV laser, a second laser system with excitation wavelength tunable from 285 nm to 320 nm was also used as an excitation source. This second laser system consisted of a cavity-dumped dye laser with 6G dye solutions, which was pumped by a YAG laser with a frequency doubler, while the output of the dye laser was frequency doubled again to provide a tunability from 285 – 320 nm [11]. This was to check the differences in PL spectral shapes due to the variation in optical absorption depth as a result of the use of different excitation wavelengths. In general, the PL results of GaN-rich alloys obtained by the two laser systems of different excitation wavelengths were similar.

## 3. Results and Discussions

### 3.1 Photoluminescence Studies of Undoped AlGa<sub>x</sub>N Epilayers

Low-temperature (10 K) cw PL spectra of Al<sub>x</sub>Ga<sub>1-x</sub>N alloys with  $x=0.3, 0.5,$  and  $0.7$  are presented in Fig. 1(a) [12]. The PL peak position ( $E_p$ ), the full width at half maximum (FWHM) as well as integrated intensity ( $S$ ) are also indicated in the figure. Besides the shift of the peak position towards shorter wavelength with increasing Al-content, one also notices a considerable decrease in the PL intensity and increase in the full width at half maximum (FWHM), which is caused by the reduction in crystalline quality as well as alloy broadening. The solid lines are the least-squares fits of data with two peaks of Gaussian distributions. With longitudinal optical (LO) phonon energies around 112 and 92 meV for AlN and GaN, respectively [13], the low energy shoulders in Fig. 1(a) are assigned to LO phonon replica of the main emission peak. An efficient way to investigate the quality of semiconductor alloy systems is by studying the linewidths of their excitonic photoluminescence spectra at low temperatures. Theoretically, higher is the quality of the alloy; closer are the excitonic photoluminescence linewidths to the theoretically predicted values [14]. It was found that the values of the excitonic linewidths we measured agree very well with those calculated using a model in which the broadening effect is assumed to be due to compositional disorder in completely random semiconductor alloys. This is illustrated in Fig 1(b), which displays the variation of the exciton emission linewidth ( $\sigma$ ) as a function of Al concentration. We found that the measured values of  $\sigma$  agree rather well with the calculated values, thus suggesting a high quality of our samples and that random compositional disorder is the main broadening mechanism in AlGa<sub>x</sub>N alloys [14].

Fig. 2(a) shows the Arrhenius plots of the PL emission intensity of Al<sub>x</sub>Ga<sub>1-x</sub>N alloys with  $x=0.3, 0.5,$  and  $0.7$ . The solid lines are the least squares fit of data with equation

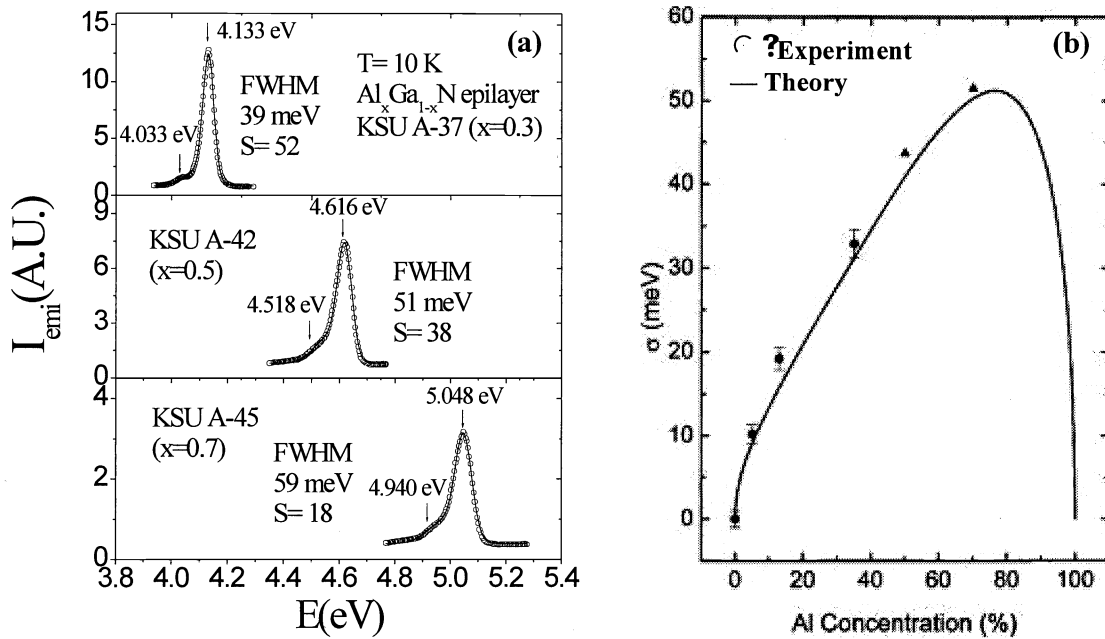


Fig. 1. (a) Photoluminescence spectra of Al<sub>x</sub>Ga<sub>1-x</sub>N alloys measured at 10 K for different Al concentrations  $x = 0.3, 0.5,$  and  $0.7$  measured at 10 K. (b) Variation of excitonic emission linewidth as a function of Al concentration: theoretical calculation (solid line), determined from the line shape analysis of the PL spectra measured at 10 K (triangles and circles). The constant value of the inhomogeneous broadening at  $x = 0$  has been subtracted from the data, so as to consider only the effect of the compositional disorder. [after Refs. 12 & 14]

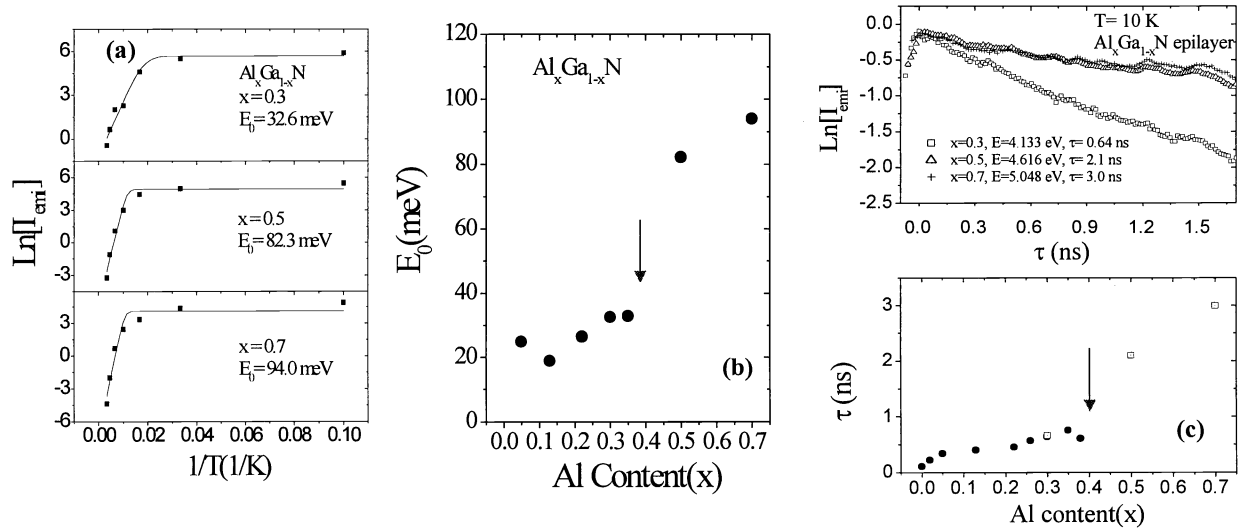


Fig. 2(a) Arrhenius plots of PL intensity for undoped AlGa<sub>1-x</sub>N alloys with  $x=0.3, 0.5,$  and  $0.7$ . The solid lines are the least squares fit of data with Eq. (1). The fitted activation energy,  $E_0$ , is also indicated in the figure. (b) The activation energy  $E_0$  as a function of Al composition  $x$ . A drastic increase of  $E_0$  is evident at  $x \sim 0.4$ . (c) Temporal responses of the PL emissions from undoped Al<sub>x</sub>Ga<sub>1-x</sub>N alloys with  $x=0.3, 0.5,$  and  $0.7$  measured at 10 K and the Al content dependence of the measured decay lifetime of Al<sub>x</sub>Ga<sub>1-x</sub>N alloys at 10 K. [after Ref. 12]

$$I_{\text{emi}}(T) = I_0 / [1 + C \exp(-E_0/kT)], \quad (1)$$

where  $E_0$  is the activation energy of the PL emission intensity, which is correlated with the carrier localization energy induced by compositional disorder. The fitted activation energy  $E_0$  is indicated in the figure. Fig. 2(b) plots the Al composition ( $x$ ) dependence of the activation energy ( $E_0$ ). The most intriguing result is that  $E_0$  has a sharp increase at  $x \sim 0.4$ . For  $x > 0.5$ ,  $E_0$  is as large as 90 meV and is much larger than the thermal energy at room temperature (25 meV).

**Table 1. Resistivity vs  $x$  in undoped  $\text{Al}_x\text{Ga}_{1-x}\text{N}$  [after Ref. 12]**

Al content $x$	Resistivity $\rho$ ( $\Omega\text{cm}$ )
0.3	0.18
0.35	2.1
0.4	190
0.45	374
0.5	$>10^5$

Time-resolved PL spectra have been measured at 10 K. Fig. 2(c) displays the Al composition ( $x$ ) dependence of the recombination lifetime. It clearly shows an increase of decay lifetime with increasing Al content and that the decay lifetime shows exactly the same trend as that of the activation energy of the PL emission intensity. The PL decay lifetime is expected to increase with the carrier/exciton localization energy [15,16]. There are many important consequences for large  $E_0$  for  $x$  greater than 0.4. Larger  $E_0$  implies larger carrier/exciton localization energies, which we believe accounts partly for the low conductivities of AlGaN alloys of high Al contents - a fact has been known for Al-rich AlGaN alloys for many years [17]. We have measured the conductivity of a set of undoped AlGaN alloys with  $x$  between 0.3 and 0.5 and the results are shown in Table 1, from which we see that the resistivity increases by about 3 orders of magnitude when Al contents increased from 0.3 to 0.4. It becomes a highly resistive material at  $x$  around 0.5 for undoped  $\text{Al}_x\text{Ga}_{1-x}\text{N}$  alloys. The resistivity results further corroborate the optical data presented in Figs. 2.

Our results thus strongly suggested that a sharp increase of the carrier localization energy in undoped high Al content AlGaN alloys is responsible for all the behaviors reported here. These include sharp increase of (a) PL emission intensity activation energy, (b) PL decay lifetime, and (c) resistivity, for undoped  $\text{Al}_x\text{Ga}_{1-x}\text{N}$  alloys at  $x$  around 0.4.

### 3.2 Achieving Highly Conductive $\text{Al}_x\text{Ga}_{1-x}\text{N}$ Alloys with High Al Contents

We have investigated the MOCVD growth of n-type  $\text{Al}_x\text{Ga}_{1-x}\text{N}$  alloys by Si-doping [18]. By examining the electrical and optical properties of vast numbers of AlGaN samples grown under different conditions, we concluded that (i) the conductivity of  $\text{Al}_x\text{Ga}_{1-x}\text{N}$  alloys continuously increases with an increase of Si doping level for a fixed value of Al content and (ii) there exists a critical Si-dopant concentration of about  $1 \times 10^{18} \text{ cm}^{-3}$  that is needed to convert insulating  $\text{Al}_x\text{Ga}_{1-x}\text{N}$  alloys with high Al contents ( $x \geq 0.4$ ) to n-type. This is illustrated in Fig. 3(a), which shows the free electron concentration ( $n$ ), mobility ( $\mu$ ), conductivity  $\sigma$  of Si-doped  $\text{Al}_x\text{Ga}_{1-x}\text{N}$  alloys as functions of the Si dopant concentration ( $N_{\text{Si}}$ ) for three different Al compositions,  $x = 0.4, 0.45, \text{ and } 0.5$ . The results clearly reveal that there exists a critical Si-dopant concentration for converting insulating  $\text{Al}_x\text{Ga}_{1-x}\text{N}$  ( $x \geq 0.4$ ) to n-type and the critical dopant concentration is about  $1 \times 10^{18} \text{ cm}^{-3}$ . We believe that this is a direct consequence of electrons filling the localized states in  $\text{Al}_x\text{Ga}_{1-x}\text{N}$  alloys caused by compositional disorder. Our results thus indicated that the density of the localized states in  $\text{Al}_x\text{Ga}_{1-x}\text{N}$  alloys with  $x \geq 0.4$  below the mobility edge (energy that separates the localized states from the extended states) is on the order of  $1 \times 10^{18} \text{ cm}^{-3}$ .

We also observe a considerable increase in the PL emission intensity with increasing  $N_{\text{Si}}$ . The improvement of optical quality by Si doping has been observed previously in GaN epilayers [19-21] and AlGaN/GaN multiple quantum wells [22]. The relative PL intensities for Si-doped  $\text{Al}_x\text{Ga}_{1-x}\text{N}$  alloys increase by about one order of magnitude when the Si doping concentration is varied from 0 to  $5 \times 10^{18} \text{ cm}^{-3}$ . For example, for  $x = 0.45$ , the relative PL emission intensity increases from 5 to 37 and to 44 as the doping concentration increases from 0 to  $1 \times 10^{18} \text{ cm}^{-3}$  and to  $5 \times 10^{18} \text{ cm}^{-3}$ . We have also measured the carrier localization energy and recombination lifetime as functions of Si doping for representative n-type  $\text{Al}_x\text{Ga}_{1-x}\text{N}$  epilayers with different Si doping levels up to  $5 \times 10^{18} \text{ cm}^{-3}$ , as we have done for the undoped  $\text{Al}_x\text{Ga}_{1-x}\text{N}$  layers. The recombination lifetime  $\tau$  and activation energy  $E_0$  of PL emission for Si-doped  $\text{Al}_{0.45}\text{Ga}_{0.55}\text{N}$  epilayers as functions of doping level are plotted in Fig. 3(b). Both values of  $\tau$  and  $E_0$  exhibit initial sharp decreases when the Si doping concentration is increased from  $N_{\text{Si}} = 0$  to  $N_{\text{Si}} = 1 \times 10^{18} \text{ cm}^{-3}$ , followed by gradual decreases as  $N_{\text{Si}}$  is further increased. These results suggest that Si-doping reduces the carrier localization effect with a sharp reduction in carrier localization energy taking place at around  $N_{\text{Si}} = 1 \times 10^{18} \text{ cm}^{-3}$ . The results shown in Fig. 3(b) thus corroborate the electrical data presented in Fig. 3(a). Our results suggest that the critical Si-doping concentration needed to fill up the localized states in  $\text{Al}_x\text{Ga}_{1-x}\text{N}$  alloys ( $x \geq 0.4$ ) is around  $N_{\text{Si}} = 1 \times 10^{18} \text{ cm}^{-3}$ , above which carriers are able to transport via extended states and reasonable conductivities can be achieved. Therefore in order to obtain good n-type conductivities in  $\text{Al}_x\text{Ga}_{1-x}\text{N}$  alloys ( $x \geq 0.4$ ), Si doping levels above  $1 \times 10^{18} \text{ cm}^{-3}$  are required.

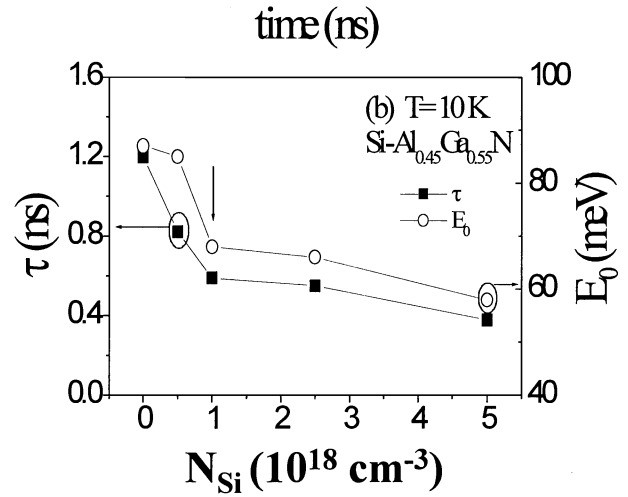
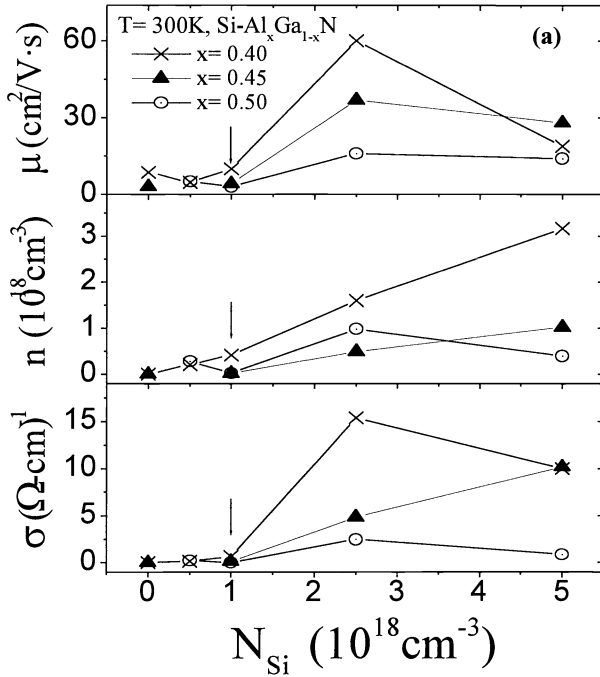


Fig. 3 (a) The free electron concentration ( $n$ ), mobility ( $\mu$ ), conductivity  $\sigma$  of Si-doped n-type  $\text{Al}_x\text{Ga}_{1-x}\text{N}$  alloys as functions of the Si dopant concentration ( $N_{\text{Si}}$ ) for three different Al compositions,  $x=0.4, 0.45$ , and  $0.5$ . (b) The Si dopant concentration dependence of the recombination lifetime  $\tau$  and thermal activation energy  $E_0$  of the PL emission intensity for  $\text{Al}_{0.45}\text{Ga}_{0.55}\text{N}$  alloys. [after Ref. 18]

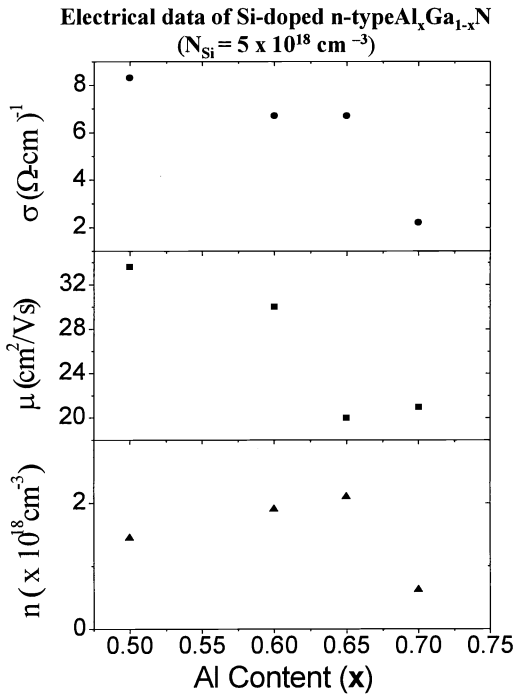


Fig. 4 The free electron concentration ( $n$ ), mobility ( $\mu$ ), conductivity  $\sigma$  of Si-doped n-type  $\text{Al}_x\text{Ga}_{1-x}\text{N}$  alloys as functions of the Al content ( $x$ ) for Si dopant concentration  $N_{\text{Si}} = 5 \times 10^{18} \text{ cm}^{-3}$ . [after Ref. 18]

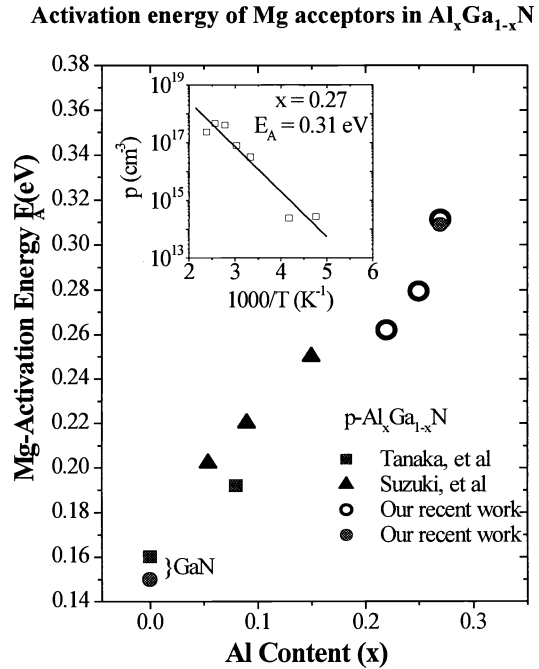


Fig. 5 Activation energy of Mg acceptors in Mg-doped p-type  $\text{Al}_x\text{Ga}_{1-x}\text{N}$  as a function of Al content  $x$ . Closed squares and triangles are data from refs. 25 and 26 respectively, while closed circles are data from our work. The inset shows the measured temperature dependence of the free hole concentration ( $p$ ) in Mg-doped p-type  $\text{Al}_{0.27}\text{Ga}_{0.73}\text{N}$  sample from which  $E_A = 0.310 \text{ eV}$  was obtained. [after Ref. 23]

$10^{18} \text{ cm}^{-3}$  is required. Indeed, by fixing the Si dopant concentration at  $5 \times 10^{18} \text{ cm}^{-3}$  while varying the growth conditions slightly, we have achieved highly conductive  $\text{Al}_x\text{Ga}_{1-x}\text{N}$  alloys with high Al contents ( $x$  up to 0.7) [18]. The Hall data for this new batch of samples are summarized in Fig. 4. Conductivity values of  $6.7 \Omega^{-1}\text{cm}^{-1}$  and  $2.2 \Omega^{-1}\text{cm}^{-1}$ , respectively, have been achieved for  $\text{Al}_{0.65}\text{Ga}_{0.35}\text{N}$  and  $\text{Al}_{0.7}\text{Ga}_{0.3}\text{N}$  alloys. We believe that the n-type conductivity values we have achieved here for  $\text{Al}_x\text{Ga}_{1-x}\text{N}$  alloys ( $x$  up to 0.7) are sufficiently high for deep UV emitter applications.

### 3.3 Properties of p-type AlGa<sub>x</sub>N Epilayers

We have investigated the MOCVD growth and optical and electrical properties of Mg-doped  $\text{Al}_x\text{Ga}_{1-x}\text{N}$  alloys. Electrical studies have revealed that we have achieved p-type conduction in  $\text{Al}_x\text{Ga}_{1-x}\text{N}$  epilayers for  $x$  up to 0.27 [23]. PL emission lines due to band-to-impurity transitions of free electrons with neutral Mg acceptors in  $\text{Al}_x\text{Ga}_{1-x}\text{N}$  alloys have been observed, from which the values of the Mg acceptor activation energy  $E_A$  were deduced and were found to increase with an increase of Al content. These were found to match very well with those obtained by Hall measurements.

The Mg-doped p-type  $\text{Al}_x\text{Ga}_{1-x}\text{N}$  epitaxial layers of thickness  $1 \mu\text{m}$  were grown on sapphire substrates with a 30 nm GaN buffer layers. For Mg-doping, bis-cyclopentadienyl-magnesium ( $\text{Cp}_2\text{Mg}$ ) was transported into the growth chamber with ammonia during growth. Postgrowth annealing at  $950^\circ\text{C}$  in nitrogen gas ambient for 8 sec resulted in p-type conduction, as verified by Hall measurements. After a further anneal at  $600^\circ\text{C}$  for 2 min in nitrogen gas, the recombination of free electrons with neutral Mg acceptor was observed to be the dominant emission lines at room temperature in  $\text{Al}_x\text{Ga}_{1-x}\text{N}$ . The emission peaks were observed at 3.615 eV, 3.667 eV and 3.682 eV for  $x = 0.22, 0.25$  and  $0.27$  respectively, from which the activation energy  $E_A(x)$  of the ionized Mg impurity in  $\text{Al}_x\text{Ga}_{1-x}\text{N}$  can be deduced simply by the difference between the energy gap  $E_g(x)$  and the observed band-to-impurity emission peak  $E(e^-, A^0)$ .  $E_g(x)$  can be estimated from the expression

$$E_g(x) = (1-x)E_{g,\text{GaN}} + xE_{g,\text{AlN}} - bx(1-x) \quad (2)$$

and  $E_A(x) = E_g(x) - E(e^-, A^0)$ . In the above expression, we use widely accepted value of the energy gap for GaN,  $E_{g,\text{GaN}} = 3.42$  eV, for AlN,  $E_{g,\text{AlN}} = 6.20$  eV and of the bowing parameter  $b = 0.90$  [24]. With these,  $E_A$  values of 0.262 eV, 0.279 eV and 0.311 eV corresponding to Al contents 0.22, 0.25 and 0.27, respectively, are obtained. It is expected that different choices of the bowing parameter  $b$  would result in variations in the  $E_A$  values. However, because the Mg acceptor level in AlGa<sub>x</sub>N alloys is quite deep, the uncertainties in  $E_A$  values due to different choices of  $b$  are not very significant. For example, the above optically determined  $E_A$  values from Eq. (2) will be reduced by about 17 - 20 meV if the bowing parameter  $b = 1$  is used. The value of  $E_A$  we obtained in the above manner are plotted as a function of Al content  $x$  in Fig. 5, together with those reported previously [25,26], all obtained by means of variable temperature Hall measurements.

Also shown in this figure are data points for p-GaN and for p- $\text{Al}_{0.27}\text{Ga}_{0.73}\text{N}$  where we determined  $E_A$  by variable temperature Hall measurements (0.15 eV and 0.309 eV respectively). The measured temperature dependence of Hall concentration ( $p$ ) in the Mg-doped p-type  $\text{Al}_{0.27}\text{Ga}_{0.73}\text{N}$  sample is shown in the inset of Fig. 8, from which a value  $E_A = 0.310$  eV was obtained. Since the hole concentrations in AlGa<sub>x</sub>N alloys are relatively low and impurity band formation is not likely, our results of  $E_A$  deduced from the PL spectra match quite well with those obtained by Hall measurements. The results shown in the inset of Fig. 5 demonstrated conclusively that we have obtained p-type  $\text{Al}_x\text{Ga}_{1-x}\text{N}$  epilayers with  $x$  up to 0.27. A hole concentration of about  $7 \times 10^{16} \text{ cm}^{-3}$  and mobility  $3 \text{ cm}^2/\text{Vs}$  at room temperature have been achieved in Mg-doped  $\text{Al}_{0.27}\text{Ga}_{0.73}\text{N}$  epilayers.

The increase of  $E_A$  with increase in band gap energy for the III-nitrides has been reported previously in other studies [25-27] and is predicted by the effective mass theory [28-30]. As a comparison with our results, the value of  $E_A$  estimated from the effective mass theory for  $x = 0.25$  for example, is between 0.263 and 0.294 eV which agrees well with the measured value of 0.279 eV. From the measured  $E_A$  versus  $x$  in Mg-doped p-type  $\text{Al}_x\text{Ga}_{1-x}\text{N}$ , the resistivity versus  $x$  can be estimated as follows:

$$\rho(\text{Al}_x\text{Ga}_{1-x}\text{N}) = \rho_0 \exp(E_A/kT) = \rho_0 \exp\{[E_A(\text{GaN}) + \Delta E_A]/kT\} = \rho(\text{GaN})\{\exp(\Delta E_A/kT)\} \quad (3)$$

where  $\Delta E_A = E_A(\text{Al}_x\text{Ga}_{1-x}\text{N}) - E_A(\text{GaN})$  and our p-type GaN has typical resistivity,  $\rho(\text{GaN})$ , of about  $1.0 \Omega\text{-cm}$ . From Eq. (3), the resistivity of  $\text{Al}_x\text{Ga}_{1-x}\text{N}$  alloys with higher values of  $x$  can be deduced. For example, if the trend in Fig. 8 holds for higher  $x$ , at Al content  $x = 0.45$ , the activation energy  $E_A$  is estimated to be 0.4 eV and the estimated resistivity should be as high as  $2.2 \times 10^4 \Omega\text{-cm}$ . This deepening of the Mg activation energy with Al content presents a real challenge for obtaining p-type AlGa<sub>x</sub>N with high Al contents.

### 3.4 Delta-doping for Enhanced P-type Conduction in GaN and Al<sub>x</sub>Ga<sub>1-x</sub>N Alloys

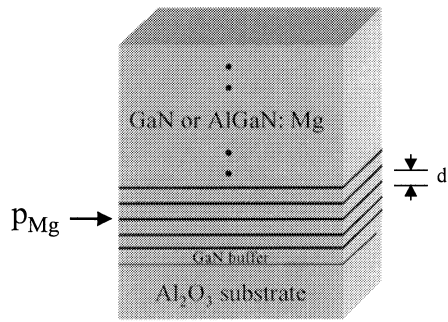


Fig. 6 Schematic diagram of Mg  $\delta$ -doped GaN or AlGaIn, where  $d$  (=15 nm) and  $P_{Mg}$  denote, respectively, the distance between two  $\delta$ -planes and the two dimensional (2D) Mg doping concentration.

MOCVD allows the growth of mono-atomic layers, which makes the impurity doping within a single atomic layer ( $\delta$ -doping) possible. Fig. 6 is a schematic diagram of Mg- $\delta$ -doped GaN or AlGaIn epilayer. A  $\delta$ -junction-like doping profile is implemented by interrupting the usual crystal-growth mode by closing the Ga (and Al) flow and leaving the N (NH<sub>3</sub>) flow continuously. The N-stabilized crystal surface is thus maintained while the Mg impurities are introduced into the growth chamber so that an impurity-growth mode results. In this mode the host crystal does not continue to grow. It is hoped that by using this technique, a small fraction of available Ga sites in the  $\delta$ -doped plane, typically  $1/10$  to  $1/10000$ , will be occupied by Mg impurities. The enhancement of n-type conduction in highly doped GaAs using Si- $\delta$ -doping in GaAs has been demonstrated previously for MBE growth [31,32]. An order of magnitude enhancement in electron concentration has been achieved in GaAs by  $\delta$ -doping over uniform doping. This technique has also been applied to GaAs/AlGaAs heterojunction field effect transistors (HFETs) for enhanced performance [33]. The distinguished feature found in Si  $\delta$ -doped GaAs was the enhancement of the electron conductivity at high doping concentration [34].

Delta doping has been proposed to reduce the complex-type compensating defects and to increase the  $p$ -type doping level in II-VI wide bandgap semiconductors in which  $p$ -type doping is also a well known difficult issue [35,36]. A high  $p$ -type doping level of  $1.5 \times 10^{18} \text{ cm}^{-3}$  was successfully achieved in ZnBeSe epilayers by  $\delta$ -doping [37].

Recently, by employing Si- $\delta$ -doping in the barrier region of AlGaIn/GaN heterojunction field effect transistor (HFET) structures, we have observed improved DC performances, i.e., enhanced maximum current, reduced leakage current, and increased breakdown voltage in Si- $\delta$ -doped structures over those of uniformly doped ones [38].

We have carried out investigations in Mg- $\delta$ -doping in GaN and AlGaIn and obtained extremely promising results [39]. We have observed that  $\delta$ -doping significantly suppresses the dislocation density in GaN and AlGaIn epilayers. This is illustrated in Fig. 7, where AFM and SEM morphologies of etched layers of Mg- $\delta$ -doped and uniformly Mg-doped Al<sub>0.07</sub>Ga<sub>0.93</sub>N epilayers are shown. The results clearly demonstrate a significant reduction of dislocation density (or etch pit density) in  $\delta$ -doped  $p$ -type Al<sub>0.07</sub>Ga<sub>0.93</sub>N. The AFM images shown in Fig. 7 indicate that the etch pit density decreased by almost one order of magnitude from  $7.9 \times 10^7 \text{ cm}^{-2}$  in uniformly Mg-doped layer to  $0.9 \times 10^7 \text{ cm}^{-2}$  in Mg- $\delta$ -doped layer. The SEM images in Fig. 7 reveal a reduction of etch pit density from  $9.4 \times 10^7 \text{ cm}^{-2}$  in uniformly Mg-doped  $p$ -type Al<sub>0.07</sub>Ga<sub>0.93</sub>N layer to  $1.8 \times 10^7 \text{ cm}^{-2}$  in Mg- $\delta$ -doped  $p$ -type Al<sub>0.07</sub>Ga<sub>0.93</sub>N layer. The results thus strongly suggest that  $\delta$ -doping can reduce dislocation density and hence improve the overall material quality of III-nitrides in general, which will be extremely beneficial to the fabrication of optoelectronics and photonics devices, especially UV emitters. We believe that the observed reduction in dislocation density is due to the growth interruption in the Mg- $\delta$ -doping duration. Ga or Al atoms are halted during  $\delta$ -doping, which stops the growth of GaN or AlGaIn. It is known that growth interruption generally reduces the dislocation densities due to the partial termination of dislocation propagation in the growth direction.

Additionally, Mg- $\delta$ -doped GaN and AlGaIn epilayers exhibit much improved electrical properties over uniformly doped layers. For GaN, we have achieved a room temperature  $p$ -type resistivity of Mg- $\delta$ -doped  $p$ -GaN epilayers as low as  $0.6 \text{ } \Omega\text{cm}$  (free hole concentration around  $2 \times 10^{18} \text{ cm}^{-3}$  and mobility around  $5 \text{ cm}^2/\text{Vs}$ ), while uniformly Mg-doped GaN epilayers typically exhibit a  $p$ -type resistivity greater than  $1 \text{ } \Omega\text{cm}$ . It was observed that the Mg- $\delta$ -doping enhances only the hole concentration and induces no changes in the hole mobility. Similar results have been obtained for  $p$ -type AlGaIn alloys. We plot the comparison results of the temperature dependent resistivity of uniformly Mg-doped and Mg- $\delta$ -doped  $p$ -type Al<sub>0.07</sub>Ga<sub>0.93</sub>N epilayers in Fig. 8(a), which demonstrates a 2-fold reduction of resistivity at room temperature by employing Mg- $\delta$ -doping. Furthermore, the measured Mg acceptor activation energy ( $E_A$ ) was also reduced from 180 meV in uniformly Mg-doped  $p$ -type Al<sub>0.07</sub>Ga<sub>0.93</sub>N to 160 meV in Mg- $\delta$ -doped  $p$ -type Al<sub>0.07</sub>Ga<sub>0.93</sub>N, which may be attributed to the enhanced free hole concentrations in Mg- $\delta$ -doped  $p$ -type Al<sub>0.07</sub>Ga<sub>0.93</sub>N. However, the results shown in the inset of Fig. 8(a) could also mean that the conduction mechanism is modified in Mg- $\delta$ -doped  $p$ -type layers over the uniformly doped layers. We have also carried out preliminary studies of the vertical transport properties of Mg- $\delta$ -doped  $p$ -type layers, which are more critical to the performance of UV emitters. Our preliminary results obtained on  $p$ -type GaN shown in Fig. 8 (b) have shown that we could obtain a 5-fold reduction in vertical resistivity in Mg- $\delta$ -doped  $p$ -type layers compared with uniformly Mg-doped  $p$ -type layers.

## AFM & SEM Images of p-AlGaN epilayers (after 0.5 $\mu\text{m}$ removal)

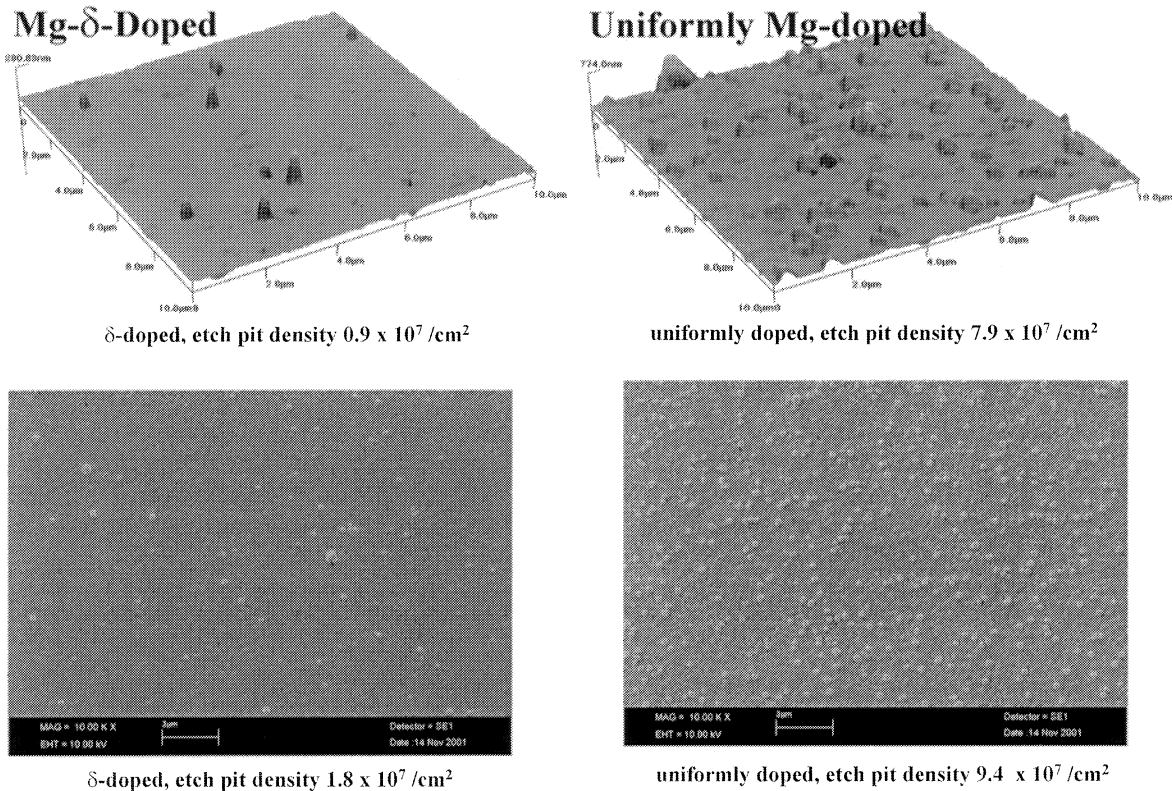


Fig. 7 AFM and SEM morphologies of etched surfaces of p-type AlGaN epilayers after a 0.5  $\mu\text{m}$  removal by inductive-coupled plasma (ICP) etching. Top: images of Mg- $\delta$ -doped and uniformly Mg-doped p-type AlGaN epilayers. Bottom: SEM images of Mg- $\delta$ -doped and uniformly Mg-doped p-type AlGaN epilayers. AFM and SEM images reveal that the etch pit density was significantly reduced in Mg- $\delta$ -doped p-type AlGaN compared with uniformly Mg-doped p-type AlGaN, implying a reduction of the dislocation density in Mg- $\delta$ -doped p-type AlGaN.

Furthermore, comparison measurements for the PL emission spectra of Mg- $\delta$ -doped and uniformly Mg-doped GaN and AlGaN epilayers have also been carried out. The PL emission intensities associated with the band-to-impurity transition line, as well as with the exciton bound to acceptor transition line ( $I_1$  around 3.44 eV for GaN and 3.57 eV for AlGaN) [40,41], are enhanced in Mg- $\delta$ -doped layers, pointing to a reduction of non-radiative recombination centers. This corroborates the results shown in Figs. 7 – dislocation density is reduced in Mg- $\delta$ -doped epilayer layers. Thus, all of our experimental data, including electrical, optical and structural data, imply that Mg- $\delta$ -doping improves not only the p-type conduction, but also the overall quality of III-nitride films.

In addition to the reduction of dislocation density giving rise to a more efficient doping, we believe that auto-compensation of Mg impurities is also reduced in Mg- $\delta$ -doped layers. Due to the relatively large Mg ionization energy in p-type GaN of about 160 mV, only about 1% of the Mg impurities are ionized at room temperature. Therefore, high doping incorporation of Mg impurities around  $10^{20} \text{ cm}^{-3}$  is a routine practice in nitride optoelectronic and electronic device structures. Self-compensation is more likely under the condition of high Mg doping levels. During the  $\delta$ -doping process, however, the Mg impurity incorporation process is modified compared with that of uniform doping. Since the Ga (and Al) atoms supply is halted, Mg impurities are more likely to replace the Ga or Al atoms during the  $\delta$ -doping process. This would reduce Mg impurity self-compensation and enhance hole concentrations in Mg- $\delta$ -doped GaN and AlGaN.

It has been demonstrated recently by several groups that incorporating Mg-doped AlGaN/GaN superlattice structure into devices could enhance the hole conduction in the lateral direction [42-44]. However, the enhancement of hole

conduction in the vertical direction by employing superlattice structure is limited because a superlattice structure simultaneously introduces potential barriers for hole conduction in the vertical direction due to the presence of higher bandgap materials. On the contrary,  $\delta$ -doping does not introduce any potential barriers in the vertical direction and is expected to enhance the vertical transport as well as the lateral transport of holes.

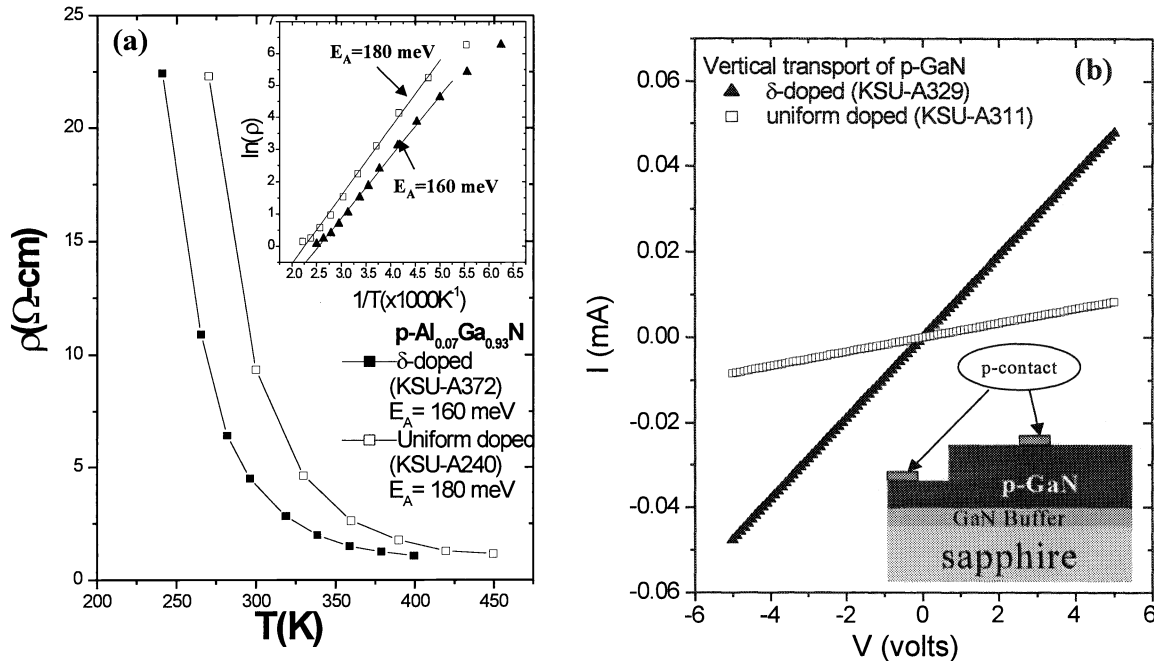


Fig. 8 (a) Resistivity ( $\rho$ ) of representative uniformly Mg-doped and Mg- $\delta$ -doped p-AlGa<sub>0.93</sub>N epilayers as functions of temperature. The inset is the Arrhenius plots of the resistivity, which indicates that  $\delta$ -doping reduces the activation energy of Mg acceptors in AlGa<sub>0.93</sub>N. (b) Comparison of “quasi” vertical transport properties of Mg uniformly doped and Mg- $\delta$ -doped p-type GaN. Etching depth (0.5  $\mu$ m) and p-type Ohmic-contact geometry were nominally identical for the two samples, as accomplished by ICP etching and photolithography patterning. A 5-fold reduction in vertical resistivity was observed in Mg- $\delta$ -doped p-type layers compared with uniformly Mg-doped p-type layers.

### 3.6 Achieving High Optical Quality AlN Epilayers

Because of our unique optical characterization capability, recently we have also successfully grown AlN epilayers on sapphire with high optical quality. For the first time, we have produced AlN epilayers that emit band-edge PL transition lines [45]. Figure 9 (a) compares the low temperature (10 K) PL spectra of our AlN and GaN epilayers covering a broad spectral range from 2.2 to 6.2 eV for AlN and 1.8 to 3.6 eV for GaN. One can see that the peak emission intensity of the deep level impurity related transition at 2.16 eV (the yellow line) in GaN epilayers is about four orders of magnitude lower than that of the band-edge transition at about 3.48 eV, revealing the high optical quality of our GaN epilayers. In AlN, there are two broad emission bands related with deep level impurities at about 2.94 and 4.36 eV, however with peak (integrated) emission intensity being only 1% (3%) of that of the band-edge emission line at 6.033 eV, which indicates that the optical quality of our AlN epilayers is also sufficiently high. It was observed that the optical quality or the intensity ratio of the band-edge to the deep level impurity transitions depends strongly on the growth conditions.

Figure 9 (b) compares the room temperature PL spectra of AlN and GaN epilayers, again covering broad spectral ranges. One sees that at room temperature the PL emission intensity of the deep level impurity related transition is also about 2 orders of magnitude lower than that of the band-edge transition in our AlN epilayers. This points to a much-improved optical quality of our AlN epilayers over those in previous cathodoluminescence (CL) studies, in which a comparable peak emission intensity for the deep level impurity related and the band-edge transition lines was observed in AlN grown on sapphire substrates [46,47]. It is interesting to note from Fig. 13 that although the 10 K band-edge emission intensity is about one order of magnitude lower in AlN than in GaN, the room temperature emission intensities are comparable for both compounds. This implies that the thermal quenching of PL emission intensity is greatly reduced in AlN over GaN, which

suggests that the detrimental effects of impurities and dislocations or non-radiative recombination channels on the quantum efficiency in AlN is much less severe than in GaN. This points to the great potential of AlN for many device applications, because it is already well known that the detrimental effect of dislocations/impurities in GaN is much smaller than in other III-V and II-VI semiconductors. Time-resolved PL measurements revealed that the recombination lifetimes of the donor bound exciton ( $I_2$ ) and free exciton transitions in AlN epilayers were around 80 ps and 50 ps, respectively. The temperature dependencies of the free exciton radiative decay lifetime and emission intensity were investigated, from which a value of about 80 meV for the free exciton binding energy in AlN epilayer was deduced. This value is believed to be the largest free exciton binding energy ever reported in semiconductors, implying excitons in AlN are an extremely robust system that would survive well above room temperature [48]. This together with other well-known physical properties of AlN may considerably expand future prospects for the application of III-nitride materials.

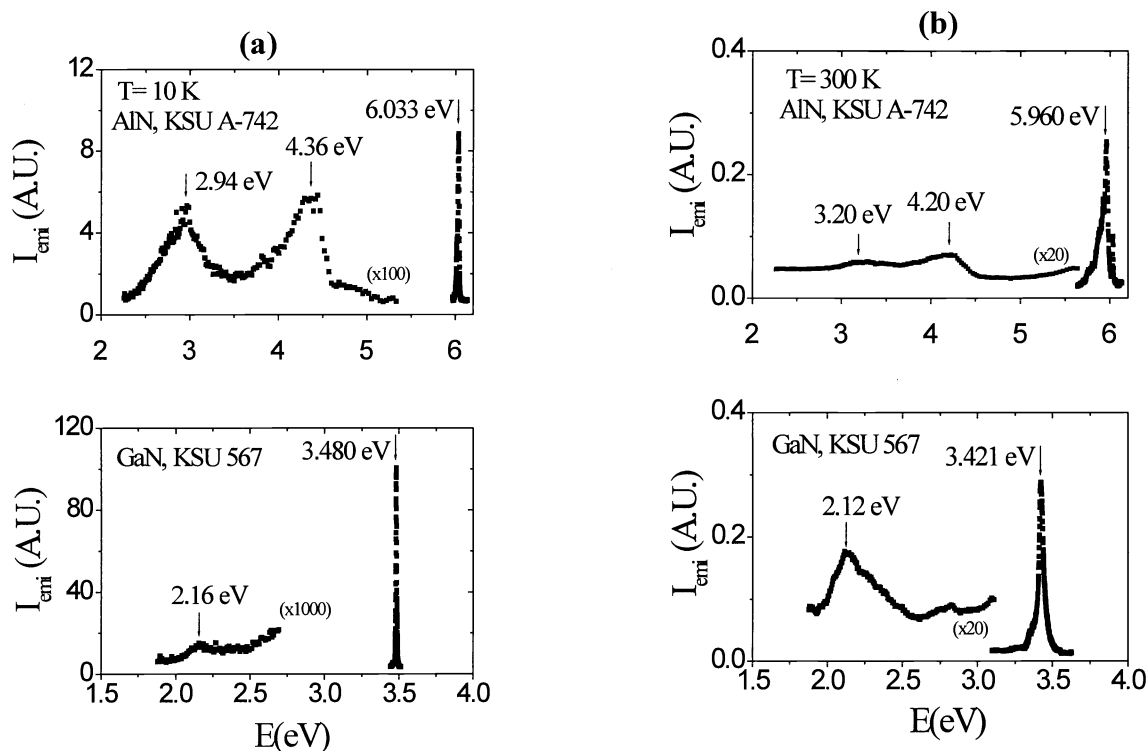


Fig. 9 PL spectra of AlN and GaN epilayers measured at (a) 10 K and (b) 300 K, which cover broad spectral ranges to include both the band-edge and deep level impurity transitions. [after Ref. 46]

In the past, AlN is referred as a ceramic due to its very large bandgap, poor quality, and highly insulating nature and is considered useful as a semiconductor only when alloyed with GaN or used as buffer and spacer layers in nitride structures and devices. Our results show that it is now emerging as an important semiconductor material, namely AlN epilayers of high optical qualities can be achieved by MOCVD. Since it is still at a very early stage for AlN epilayer growth, significant improvements in materials quality are anticipated. Indeed, it was also shown recently that the conductivity of AlN can be controlled and n-type conduction with a free electron concentration of about  $1 \times 10^{17} \text{cm}^{-3}$  has been achieved by Si doping [49]. With the demonstrated abilities of achieving high optical quality here and the n-type conductivity control of AlN epilayers, many novel applications of III-nitrides are conceivable.

#### 4. Summary

There are many problems and questions that still stand in the way of the practical device implementation of deep UV emitters. Methods for improved material qualities as well as doping efficiencies still need to be further explored. The use of AlN bulk single crystals as substrates are expected to reduce crystal defect densities as well as UV photon absorption in UV emitter structures due to its better lattice constant and thermal expansion coefficient matches over other substrates, high thermal conductivity, and large energy gap. Thus epitaxial growth conditions for UV emitter materials and device

structures on AlN bulk substrates have to be optimized. Novel approaches for ohmic contact fabrication, p-type contacts in particular, must be further developed to curtail the problem of very low p-type conductivity in AlGaN alloys with high Al contents. A better understanding of fundamental properties of AlGaN alloys and their associated QWs with high Al contents is also essential.

#### Acknowledgements

Our research program is supported by grants from ARO, NSF, DOE, BMDO, DARPA, and ONR. This review paper is a collection of contributions from our group members: J. Li, K. H. Kim, K. B. Nam, M. L. Nakarmi, S. X. Jin, T. N. Order, and J. Shakya.

#### References:

- [1] S. Nakamura and G. Fasol, *The Blue Laser Diode*, (Springer, New York, 1997).
- [2] H. Morkoc, S. Strite, G. B. Gao, M. E. Lin, B. Sverdlov, and M. Burns, *J. Appl. Phys.* **76**, 1363 (1994).
- [3] J. R. Lakowicz, *Principles of Fluorescence Spectroscopy*, 2<sup>nd</sup> edition, (Kluwer Academic Publishers, Now York, 1999).
- [4] *Gallium Nitride*, Semiconductors and Semimetals Volume 50, Volume Editors J. I. Pankove and T. D. Moustakas, edited by R. K. Willardson and Eicke R. Weber, Academic Press 1998.
- [5] I. Akasaki and H. Amano, *Jpn. J. Appl. Phys.* **36**, 5393 (1997).
- [6] T. Tammura, T. Setomoto, and T. Taguchi, *J. Lumin.* **87-89**, 1180 (2000).
- [7] I. Akasaki and H. Amano, *Jpn. J. Appl. Phys.* **36**, 5393 (1997).
- [8] Y. Sato, N. Takahashi, and S. Sato, *Jpn. J. Appl. Phys.* **35**, L838 (1996).
- [9] F. Hide, P. Kozodoy, S. P. Denbaars, and A. J. Heeger, *Appl. Phys. Lett.* **70**, 2664 (1997).
- [10] M. A. Khan, V. Adivarahan, J. P. Zhang, C. Chen, E. Kuokatis, A. Chitnis, M. Shatalov, J. W. Yang, and G. Simin, *Jpn. J. Appl. Phys.* **40**, L1308 (2001).
- [11] <http://www.phys.ksu.edu/area/GaNgroup>.
- [12] J. Li, K. B. Nam, J. Y. Lin, and H. X. Jiang, *Appl. Phys. Lett.* **79**, 3245 (2001).
- [13] *Semiconductors-Basic Data*, 2<sup>nd</sup> revised edition, edited by Otfried Madelung (Springer, Berlin, 1996).
- [14] G. Coli, K. K. Bajaj, J. Li, J. Y. Lin, and H. X. Jiang, *Appl. Phys. Lett.* **78**, 1829 (2001) and *Appl. Phys. Lett.* **80**, 2907 (2002).
- [15] H. S. Kim, R. A. Mair, J. Li, J. Y. Lin, and H. X. Jiang, *Appl. Phys. Lett.* **76**, 1252 (2000).
- [16] G. D. Chen, M. Smith, J. Y. Lin, H. X. Jiang, M. Asif Khan, and C. J. Sun, *Appl. Phys. Lett.* **67**, 1653 (1995).
- [17] M. D. Bremser, *Gallium Nitride and Related Semiconductors*, edited by J. H. Edgar, S. Strite, I. Akasaki, H. Amano, and C. Wetzel, p. 147.
- [18] K. B. Nam, J. Li, M. L. Nakarmi, J. Y. Lin, and H. X. Jiang, *Appl. Phys. Lett.* **81**, 1038 (2002).
- [19] Xiong Zhang, Soo-Jin Chua, Wei Liu, and Kok-Boon Chong, *Appl. Phys. Lett.* **72**, 1890 (1998).
- [20] Z.Q. Li, H. Chen, H.F. Liu, L. Wan, M.H. Zhang, Q. Juang, and J.M. Zhou, *Appl. Phys. Lett.* **76**, 3765 (2000).
- [21] Sergei Ruvimov, Zuzanna Liliental-Weber, Tadeusz Suski, Joel W. Ager III, and Jack Washburn, *Appl. Phys. Lett.* **69**, 990 (1996).
- [22] K.C. Zeng, J. Y. Lin, H. X. Jiang, A. Salvador, G. Popovici, H. Tang, W. Kim, and H. Morkoc, *Appl. Phys. Lett.* **71**, 1368 (1997).
- [23] J. Li, T. N. Oder, M. L. Nakarmi, J. Y. Lin, and H. X. Jiang, *Appl. Phys. Lett.* **80**, 1210 (2002).
- [24] Y. Koide, H. Itoh, M. R. H. Khan, K. Hiramato, N. Sawaki and I. Akasaki, *J. Appl. Phys.* **61**, 4540 (1987).
- [25] T. Tanaka, A. Watanabe, H. Amano, Y. Kobayashi, I. Akasaki, S. Yamazaki and M. Koike, *Appl. Phys. Lett.* **65**, 593 (1994).
- [26] M. Suzuki, J. Nishio, M. Onomura and C. Hongo, *J. Cryst. Growth* **189/190**, 511 (1998).
- [27] K. Kumakura, T. Makimoto and N. Kobayashi, *Jpn. J. Appl. Phys.* **39**, L337 (2000).
- [28] I. Akasaki and H. Amano, *Jpn. J. Appl. Phys.* **36**, 5393 (1997).
- [29] J. B. Xia, K. W. Cheah, X. L. Wang, D. Z. Sun and M. Y. Kong, *Phys. Rev. B* **59**, 10119 (1999).
- [30] F. Mireles and S. E. Ulloa, *Phys. Rev. B* **58**, 3879 (1998).
- [31] C.E.C. Wood, G. Metze, J. Berry, and L. F. Eastman, *J. Appl. Phys.* **51**, 383 (1980).
- [32] E.F. Schubert, J.E. Cunningham, W.T. Tsang, and T.H. Chiu, *Appl. Phys. Lett.* **49**, 232 (1986).
- [33] E.F. Schubert and K. Ploog, *Jpn. J. Appl. Phys.* **24**, L608 (1983).
- [34] E.F. Schubert, J.E. Cunningham, and W.T. Tsang, *Solid State Commun.* **63**, 591 (1987).
- [35] Z. Zhu, G. D. Brownlin, G. Horsburgh, P. J. Thompson, S. Y. Wang, K. A. Prior, and B. C. Cavenett, *Appl. Phys. Lett.* **67**, 2167 (1995).
- [36] J. L. De Miguel, S. M. Shibli, M. C. Tamargo, and B. J. Skromme, *Appl. Phys. Lett.* **53**, 2065 (1988).

- [37] S. P. Guo, W. Lin, X. Zhou, and M. C. Tamargo C. Tian, I. Kuskovsky, and G. F. Neumark, *J. of Appl. Phys.* 90, 1725 (2001).
- [38] Z. Y. Fan, J. Li, J. Y. Lin, and H. X. Jiang, *Appl. Phys. Lett.*, *Appl. Phys. Lett.* Dec. 9<sup>th</sup> issue, 2002.
- [39] M. L. Nakarmi, K. H. Kim, J. Li, J. Y. Lin and H. X. Jiang, *App. Phys. Lett.*, in press.
- [40] M. Smith, G. D. Chen, J. Y. Lin, H. X. Jiang, A. Salvador, W. Kim, O. Aktas, A. Botchkarev, and H. Morkoc, *Appl. Phys. Lett.* 68, 1883 (1996).
- [41] M. Smith, G. D. Chen, J. Y. Lin, H. X. Jiang, M. Asif Khan, and C. J. Sun, *Appl. Phys. Lett.* 67, 3295 (1995).
- [42] P. Kozodoy, M. Hansen, S. P. DenBaars, and U. K. Mishra, *Appl. Phys. Lett.* 74, 3681 (1999).
- [43] P. Kozodoy, Y. P. Smorchkova, M. Hansen, H. Xing, S. P. DenBaars, and U. K. Mishra, A. W. Saxler, P. Perrin, and W. C. Mitchel, *Appl. Phys. Lett.* 75, 2444 (1999).
- [44] H. X. Jiang, S. X. Jin, J. Li, J. Shakya, and J. Y. Lin, *Appl. Phys. Lett.* 78, 1303 (2001).
- [45] J. Li, K. B. Nam, M. L. Nakarmi, J. Y. Lin, and H. X. Jiang, *Appl. Phys. Lett.* 81, 3365 (2002).
- [46] F. R. B. Hossain, X. Tang, K. Wongchotigul, M. G. Spencer, *Proc. SPIE*, vol. 2877, p. 42, (1996).
- [47] C. M. Zettering, M. Ostling, K. Wongchotigul, M. G. Spencer, X. Tang, C. I. Harris, N. Ordell, and S. S. Wong, *J. Appl. Phys.* 82, 2990 (1997).
- [48] K.B. Nam, J. Li, M. L. Nakarmi, J. Y. Lin and H. X. Jiang, "Deep ultraviolet picosecond time-resolved photoluminescence studies of AlN epilayers," *Appl. Phys. Lett.* submitted.
- [49] Y. Taniyasu, M. Kasu, and N. Kobayashi, *Appl. Phys. Lett.* 81, 1255 (2002).